Boosting Adversarial Transferability for Skeleton-based Action Recognition via Exploring the Model Posterior Space

Yunfeng Diao[1], Baiqi Wu[1], Ruixuan Zhang[1], Xun Yang[2], Meng Wang[1], and He Wang[3]

[1] Hefei University of Technology, China
[2] University of Science and Technology of China, China
[3] University College London, UK

Abstract. Skeletal motion plays a pivotal role in human activity recognition (HAR). Recently, attack methods have been proposed to identify the universal vulnerability of skeleton-based HAR(S-HAR). However, the research of adversarial transferability on S-HAR is largely missing. More importantly, existing attacks all struggle in transfer across unknown S-HAR models. We observed that the key reason is that the loss landscape of the action recognizers is rugged and sharp. Given the established correlation in prior studies [27, 41] between loss landscape and adversarial transferability, we assume and empirically validate that smoothing the loss landscape could potentially improve adversarial transferability on S-HAR. This is achieved by proposing a new post-train Dual Bayesian strategy, which can effectively explore the model posterior space for a collection of surrogates without the need for re-training. Furthermore, to craft adversarial examples along the motion manifold, we incorporate the attack gradient with information of the motion dynamics in a Bayesian manner. Evaluated on benchmark datasets, e.g. HDM05 and NTU 60, the average transfer success rate can reach as high as 35.9% and 45.5% respectively. In comparison, current state-of-the-art skeletal attacks achieve only 3.6% and 9.8%. The high adversarial transferability remains consistent across various surrogate, victim, and even defense models. Through a comprehensive analysis of the results, we provide insights on what surrogates are more likely to exhibit transferability, to shed light on future research. The code will be shared upon acceptance.

Keywords: Skeleton-based action recognition · Transfer-based adversarial attack · Bayesian deep learning

1 Introduction

Deep learning has made remarkable progress over the past decade in various tasks. However, deep neural networks (DNNs) are vulnerable to adversarial examples, which are crafted by imposing imperceptible perturbations to benign samples [11]. Recently, the adversarial vulnerability in skeleton-based human activity recognition (S-HAR) [7, 40] has garnered attention [7, 40] due to

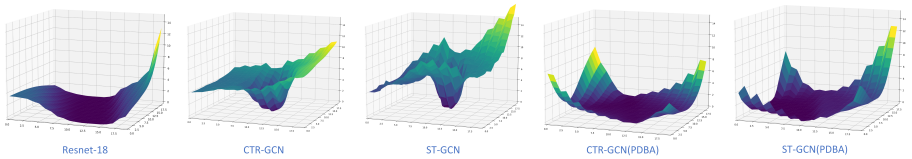

Fig. 1: Comparison of loss landscapes of trained models. Resnet-18 is trained on CIFAR-10. ST-GCN and CTR-GCN are trained on NTU60. The loss plots in each column are generated from the same original data randomly selected from the test dataset. This visualization method was proposed by [17], which approximates neural network loss functions in low-dimensional subspaces of the model's parameter space. The x axis and y axis represent two random direction vectors. The z axis represents the loss. PDBA significantly smoothens the rugged landscape.

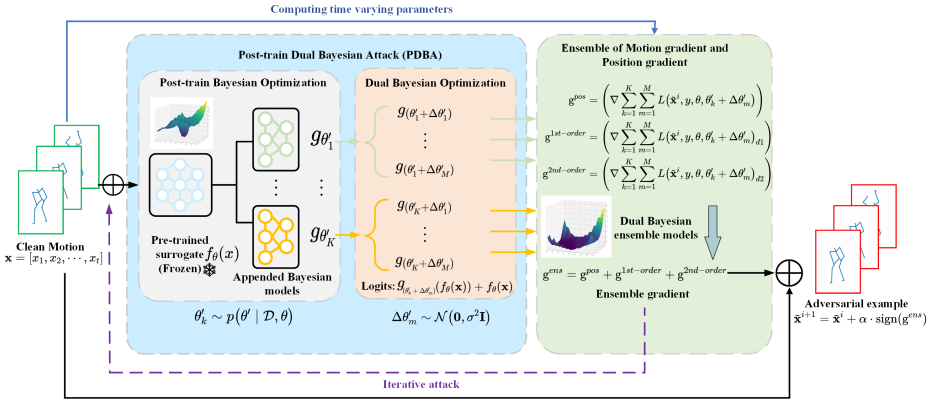

Fig. 2: An overview of PDBA.

the widespread utilization of skeletal motion in security-critical applications such as sport analysis, bio-mechanics, surveillance, and human-computer interactions [28]. Recent studies [20, 35, 36, 40] have demonstrated that adversarial examples can successfully fool skeletal classifiers when the structure and parameters of a given model are known, i.e. under the white-box setting. However, research on adversarial transferability on S-HAR has been largely unexplored. While state-of-the-art white-box [20, 40] attack or even no-box attack [24] can deliver transfer-based attacks via surrogate models, they usually exhibit a low transfer success rate, in contrast to the common belief that adversarial examples possess transferability across different model architectures and parameters [22]. This disparity prompts us to raise the following questions: *What is the primary reason that skeletal motions face challenges in exhibiting adversarial transferability compared to images? How can we overcome this challenge to improve adversarial transferability on S-HAR?*

We begin by examining the factors contributing to poor adversarial transferability on S-HAR. Current skeletal attacks typically utilize gradient-based optimization methods tailored to the unique characteristics of motion data, e.g.

motion dynamics [24, 40] and human body topology [35], or employ gradient variation such as momentum-based gradient [9]. One obvious observation is most attacks on S-HAR compute attack gradient from a *single* surrogate model, and transferability is highly sensitive to the chosen surrogate, e.g. CTR-GCN [5] as the surrogate has better transferability than ST-GCN [44] (refer to the results in Tab. 7). This observation motivates us to investigate the differences between different surrogate models. Previous research has proven that the smoothness of the loss surface is a key factor that influences the adversarial transferability [27, 41]. We hence investigate the smoothness of the loss landscape across different surrogate models. As shown in Fig. 1, 1) the loss surface of the trained models on skeleton data is generally sharper than trained models on image data. This observation provides a potential explanation for the lower adversarial transferability on S-HAR compared to image classification, despite employing the same attack strategy [9, 24]. 2) CTR-GCN has flatter regions of the loss landscape than ST-GCN. Consequently, we argue smoothening the rugged landscape of the surrogate will improve the adversarial transferability for S-HAR.

Bayesian neural networks have been shown to exhibit lower sharpness and better generalization ability [2, 25]. Therefore, attacking the entire model distribution is more likely to generalize [13, 18]. However, attacking skeletal motion in a Bayesian manner faces two challenges. First, action classifiers contain a large number of parameters, commonly at least numbering several millions. Sampling the posterior distribution for such complex models can be computationally expensive and consume a heavy memory footprint. Additionally, prior research has indicated that skeletal adversarial examples tend to lie or near the motion manifold [7]. Naively applying existing Bayesian attack would lead to a crude approximation of this manifold, as the attack gradient does not contain information of the motion dynamics. How to craft adversarial examples along the motion manifold in a Bayesian manner is a trick problem.

To tackle these challenges, we propose a new ensemble-based attack from a novel post-train Bayesian view, to explore the model posterior space for a collection of surrogates with high adversarial transferability. Unlike existing ensemble-based attacks which seek to retrain an ensemble of surrogate models, our post-train Bayesian strategy fixes the pre-trained surrogate and appends small extra Bayesian components to turn it into a Bayesian model, without the need for re-training. Specifically, we propose a dual Bayesian optimization strategy. One Bayesian sampling is to maximize the predictive distribution, while we argue that the surrogate with the best accuracy may not imply the best transferability. Therefore, our objective is to seek a collection of new surrogates around the optimal surrogates during the dual Bayesian sampling phase. We name our method Post-train Dual Bayesian Attack (PDBA). Furthermore, since the original attack gradient treats each frame as independent, ignoring the inter-frame dependencies in time, we integrate information of the motion dynamics into the Bayesian attack gradient through explicit motion modeling. An overview illustration of PDBA is shown in Fig. 2.

PDBA can circumvent model re-training, avoiding a heavy memory footprint and speeding up the training process. We extensively evaluate PDBA on several state-of-the-art classifiers across multiple datasets in both untargeted and targeted attacks. Compared with state-of-the-art S-HAR attacks, PDBA improves the average transfer success rate by 31.6% on HDM05, 35.7% on NTU 60, and 12.2% on NTU 120. More importantly, PDBA significantly improves the adversarial transferability against state-of-the-art defense models for S-HAR, conclusively showing its efficacy and versatility. By analyzing the extensive empirical results, we provide insights on what surrogates possess transferability, to shed light on future research.

2 Related Work

2.1 Skeleton-Based Human Action Recognition

S-HAR has attracted considerable attention across diverse applications [28]. In the era of deep learning, early work employed convolutional neural networks [1] and recurrent neural networks [10] to extract motion features in the spatial domain and temporal domain, respectively. Recently, graph convolutional networks (GCN) [30, 44] have showcased cutting-edge performance by representing the skeleton as a topological graph, where the nodes and edges correspond to the joints and bones respectively. To further enhance performance, there have been subsequent proposals of refined graph designs and network architectures [23, 31, 47].

2.2 Adversarial Attacks

Adversarial attacks were first introduced in [34], highlighting the susceptibility of deep neural networks and have been applied across different types of data [28]. The existing attacks are mainly divided into white-box attacks [12] and black-box attacks [3, 9, 43]. The former is given full knowledge of the architecture and parameters of a victim model, while the latter assumes that the attacker cannot access any information of the victim model, which mainly includes decision-based [3, 15] and transfer-based methods [9]. Recently, many gradient-based attacks [6, 20, 35, 36, 40] have been proposed to identify the vulnerability of S-HAR. Specifically, [20, 40] leverage perception loss to ensure the imperceptibility of the attack. Tanaka et al. [35] restrict the perturbations to the lengths of the skeleton's bones. Lu et al. [24] define a new hard no-box attack on S-HAR. Albeit identifying a key issue, these white-box and no-box methods all suffer from low transfer success rates. Diao et al. [7] propose the first decision-based S-HAR attack, but it needs a huge number of queries. In this paper, we focus on transfer-based attack. Transfer-based attacks do not need any queries on the target models, rendering them more difficult to detect by the target system. Despite the abundance of transfer-based attack methods in image classification [9, 13, 18, 19, 27, 43], research in S-HAR remains largely unexplored. To this end, we fill this gap by proposing a new transfer-based attack on S-HAR.

3 Methodology

3.1 A Bayesian Perspective on Transfer-based Attack

We denote a normal motion $\mathbf{x} \in \mathcal{X}$ and its corresponding label $y \in \mathcal{Y}$. Given a surrogate action recognizer f_θ parametrized by θ, f_θ is trained to map a motion $\mathbf{x}$ to a predictive distribution $p(y \mid \mathbf{x}, \theta)$. The white-box attack can be optimized by minimizing the predictive probability:

$$\arg\min_{\|\delta\|_p \leq \epsilon} p(y \mid \mathbf{x} + \delta, \theta) \tag{1}$$

where δ is the adversarial perturbation and ϵ is the perturbation budget. The procedure of transfer-based attack is firstly crafting the adversarial example $\mathbf{x}+\delta$ by attacking the surrogate model, then transferring $\mathbf{x} + \delta$ to directly attack the unseen target model. In Eq. (1), since the transferable adversarial examples are optimized against one surrogate model, adversarial examples with transferability heavily rely on the condition that the surrogate model learns the similar classification boundary with an unknown target model. While possible for image classification, it proves unrealistic for S-HAR [24,39]. Most of the state-of-the-art S-HAR models are based on graph convolutional network, where the definitions of skeleton topological graphs vary, resulting in significantly different learned latent features in high-dimensional space [24]. Bayesian neural networks have been demonstrated to possess lower sharpness and better generalization capability. From a Bayesian perspective, attacking BNNs can fuse outputs from an ensemble of infinitely many DNNs with diverse predictions to increase the power of adversarial transferability [13, 18]. Therefore, Eq. (1) can be reformulated by approximately minimizing the Bayesian posterior predictive distribution to improve adversarial transferability:

$$\arg\min_{\|\delta\|_p \leq \epsilon} p(y \mid \mathbf{x} + \delta, \mathcal{D}) = \arg\min_{\|\delta\|_p \leq \epsilon} \mathbb{E}_{\theta \sim p(\theta \mid \mathcal{D})} p\left(y \mid \mathbf{x} + \delta, \theta\right) \tag{2}$$

where $p(\theta \mid \mathcal{D}) \propto p(\mathcal{D} \mid \theta) p(\theta)$, in which $\mathcal{D}$ is the dataset and $p(\theta)$ is the prior of model weights.

3.2 Post-train Dual Bayesian Attack

Necessity of a Post-train Bayesian Attack Unfortunately, attacking action recognizers in such a Bayesian manner is not a straightforward task due to several factors. First, directly sampling the posterior is intractable for DNNs. Although approximate sampling is possible, such as MCMC sampling or variational inference, sampling is prohibitively slow and resource-intensive due to the high dimensionality of the sampling space (commonly at least several million parameters in action classifiers). In addition, action classifiers with a large number of parameters are normally pre-trained on large datasets [21]. It is not desirable for end-users to re-train the surrogate model. Finally, unlike ensemble-based methods that average gradients from many surrogates, which is likely to decrease the

white-box attack strength(refer to the results in Tab. 2), the post-train Bayesian strategy turns a single surrogate into a Bayesian model, effectively mitigating the trade-off between white-box and transfer-based attack performance.

To solve the above issues, we propose a new *post-train* Bayesian attack. We maintain the integrity of the pre-trained classifier while appending a tiny MLP $g_{\theta'}$ behind it, connected via a skip connection. Specially, the final output logits can be computed as: logits $= g_{\theta'}(f_\theta(\mathbf{x})) + f_\theta(\mathbf{x})$. In practice, we adopt Monte Carlo sampling to optimize the appended Bayesian model:

$$\max_{\theta'} \mathbb{E}_{\theta' \sim p(\theta'|\mathcal{D},\theta)} p\left(y \mid \mathbf{x}, \theta, \theta'\right) \approx \max_{\theta'_k} \frac{1}{K} \sum_{k=1}^{K} p\left(y \mid \mathbf{x}, \theta, \theta'_k\right), \theta'_k \sim p(\theta' \mid \mathcal{D}, \theta) \tag{3}$$

where K is the number of appended models.

f_θ is frozen when training $g_{\theta'}$, hence our post-train Bayesian strategy keeps the classifier intact and avoids re-training. More importantly, training on $g_{\theta'}$ is much faster than on f_θ because $g_{\theta'}$ is much smaller than f_θ.

Post-train Dual Bayesian Optimization In Eq. (3), we have obtained a set of θ'_k with the optimal classification performance. However, we argue that the surrogate model with the best accuracy does not imply the best transferability. For example, models adversarially trained with small perturbation budgets slightly sacrifice accuracy but improve the transferability as better surrogates [33, 46]. Therefore, we assume that around the region of optimal model parameters, there exist new surrogates with better transferability. Inspired by [18], we first assume the posterior distribution of the appended model is an isotropic Gaussian $\mathcal{N}\left(\theta', \sigma^2\mathbf{I}\right)$, because Gaussian distributions allow for analytical solutions to reduce computational complexity compared to more complicated assumptions. We will discuss a more practical assumption in the next subsection. Then Eq. (3) can be further improved by dual Bayesian optimization:

$$\max_{\theta'} \mathbb{E}_{\theta' \sim p(\theta'|\mathcal{D},\theta)} \mathbb{E}_{\Delta\theta' \sim \mathcal{N}\left(\mathbf{0}, \sigma^2\mathbf{I}\right)} p\left(y \mid \mathbf{x}, \theta, \theta' + \Delta\theta'\right) \tag{4}$$

We further use dual Monte Carlo sampling to approximate Eq. (4):

$$\min_{\theta'_k \sim p(\theta'|\mathcal{D},\theta)} \frac{1}{MK} \sum_{k=1}^{K} \sum_{m=1}^{M} L\left(\mathbf{x}, y, \theta, \theta'_k + \Delta\theta'_m\right), \Delta\theta'_m \sim \mathcal{N}\left(\mathbf{0}, \sigma^2\mathbf{I}\right) \tag{5}$$

where L is the classification loss. The dual Bayesian optimization consists of two steps. One Bayesian sampling aims to optimize θ'_k for accuracy. As we mentioned before, we argue that the surrogate with the best accuracy does not imply the best transferability. So in the dual Bayesian sampling phase, we aim to find new surrogates around the θ'_k (if $\theta' + \Delta\theta'$ too far from θ', it would reduce accuracy, resulting in a decreased number of generated transfer adversarial examples). Considering dual MCMC samplings computationally intensive, we instead consider

the worst-case parameters from the posterior, followed by [18]. Hence Eq. (5) can be equivalent to a min-max optimization problem, written as:

$$\min_{\theta'_k \sim p(\theta'|\mathcal{D},\theta)} \max_{\Delta\theta' \sim \mathcal{N}(\mathbf{0},\sigma^2\mathbf{I})} \frac{1}{K}\sum_{k=1}^{K} L\left(\mathbf{x}, y, \theta, \theta'_k + \Delta\theta'\right),\ p(\Delta\theta') \geq \xi \tag{6}$$

The confidence region of the Gaussian posterior is regulated by ξ. We discuss the sensitivity to ξ in the supplementary material. By Taylor expansion at θ', we have:

$$\min_{\theta'_k \sim p(\theta'|\mathcal{D},\theta)} \max_{\Delta\theta' \sim \mathcal{N}\left(\mathbf{0},\sigma^2\mathbf{I}\right)} \frac{1}{K}\sum_{k=1}^{K}[L\left(\mathbf{x}, y, \theta, \theta'_k\right) + \nabla_{\theta'_k} L\left(\mathbf{x}, y, \theta, \theta'_k\right)^T \Delta\theta'], p(\Delta\theta') \geq \xi \tag{7}$$

As $\Delta\theta'$ is sampled from a zero-mean isotropic Gaussian distribution, the inner maximization can be solved analytically:

$$\Delta\theta'_* = \lambda_{\xi,\sigma} \nabla_{\theta'} L\left(\mathbf{x}, y, \theta, \theta'\right) / \left\|\nabla_{\theta'} L\left(\mathbf{x}, y, \theta, \theta'\right)\right\|. \tag{8}$$

Then the gradient of $\nabla_{\theta'_k} L\left(\mathbf{x}, y, \theta, \theta'_k\right)^T \Delta\theta'$ in Eq. (7) becomes $\nabla_{\theta'_k} L\left(\mathbf{x}, y, \theta, \theta'_k\right) + \mathbf{H}\Delta\theta'_*$, in which $\mathbf{H}\Delta\theta'_*$ can be approximately estimated via the finite difference method:

$$\mathbf{H}\Delta\theta'_* \approx \frac{1}{\gamma}\left(\nabla_{\theta'_k}\frac{1}{K}\sum_{k=1}^{K} L\left(\mathbf{x}, y, \theta, \theta'_k + \gamma\Delta\theta'_*\right) - \nabla_{\theta'_k}\frac{1}{K}\sum_{i=1}^{K} L\left(\mathbf{x}, y, \theta, \theta'_k\right)\right) \tag{9}$$

where γ is a small positive constant. Therefore, our final optimization objective is:

$$\frac{1}{K}\sum_{k=1}^{K} \nabla_{\theta'_k} L\left(\mathbf{x}, y, \theta, \theta'_k\right) + (1/\gamma)\left(\nabla_{\theta'_k} L\left(\mathbf{x}, y, \theta, \theta'_k + \gamma\Delta\theta'_*\right) - \nabla_{\theta'_k} L\left(\mathbf{x}, y, \theta, \theta'_k\right)\right) \tag{10}$$

Post-train Dual Bayesian Inference Followed by [38], we use Stochastic Gradient Adaptive Hamiltonian Monte Carlo [32] for the post-train dual Bayesian optimization. In the dual sampling phase, we assume $\Delta\theta'$ is sampled from Gaussian posterior, which has a presumed isotropic covariance matrix. In practice, we follow the suggestions from [18] to calculate the mean and the covariance from data by using SWAG [25], as SWAG can offer an improved approximation to the posterior over parameters. While the posterior still relies on Gaussian approximation, it specifically incorporates the SWA [14] solution as its mean, and decomposes the covariance into a low-rank matrix and a diagonal matrix. Specifically, we compute:

$$\theta'_k \sim \mathcal{N}\left(\theta'_{k,\mathrm{SWA}}, \boldsymbol{\Sigma}_{\mathrm{SWAG}}\right), \text{ and } \boldsymbol{\Sigma}_{\mathrm{SWAG}} = \frac{1}{2}\left(\boldsymbol{\Sigma}_{\mathrm{diag}} + \boldsymbol{\Sigma}_{\text{low-rank}}\right) \tag{11}$$

Remember that the posterior discussed in the preceding section is formulated based on the worst cases, thus facilitating its effortless integration with SWAG to expand diversity and flexibility.

3.3 Motion Gradient for PDBA

Typically, PDBA can be performed with iterative gradient-based methods:

$$\tilde{\mathbf{x}}^{i+1} = \tilde{\mathbf{x}}^{i} + \alpha \cdot \text{sign}(\nabla \sum_{k=1}^{K} \sum_{m=1}^{M} L\left(\tilde{\mathbf{x}}^{i}, y, \theta, \theta'_k + \Delta\theta'_m\right)) \tag{12}$$

where α is the step size. For notational simplicity, we notate $L\left(\tilde{\mathbf{x}}^{i}, y, \theta, \theta'_k + \Delta\theta'_m\right)$ as $L\left(\tilde{\mathbf{x}}^{i}\right)$. Unlike static data like images, skeletal sequences contain rich dynamics, hence we argue only considering *position* gradient is not enough. *Position* gradient assumes each frame is independent while ignoring the dependency between frames in time. To fully represent the motion dynamics, *first-order* (velocity) and *second-order* (acceleration) gradient information should also be considered. To this end, we augment the original *position* gradient with the motion gradient $(L\left(\tilde{\mathbf{x}}^{i}\right))_{d1}$ and $(L\left(\tilde{\mathbf{x}}^{i}\right))_{d2}$, then Eq. (12) becomes:

$$\tilde{\mathbf{x}}^{i+1} = \tilde{\mathbf{x}}^{i} + \alpha \cdot \text{sign}(\nabla \sum_{k=1}^{K} \sum_{m=1}^{M} [w_1 L\left(\tilde{\mathbf{x}}^{i}\right) + w_2 (L\left(\tilde{\mathbf{x}}^{i}\right))_{d1} + w_3 (L\left(\tilde{\mathbf{x}}^{i}\right))_{d2}])) \tag{13}$$

Motion gradient can be computed by explicit modeling [42] or implicit learning [37]. Since using implicit learning needs to train another data-driven model to learn the motion manifold, thereby increasing computation overhead, we opt for explicit modeling. Specifically, we employ time-varying autoregressive models(TV-AR) [4] because TV-AR can effectively estimate the dynamics of skeleton sequences by modeling the temporary non-stationary signals [42].

Given a motion with t frames $\mathbf{x} = [x_1, x_2, \cdots, x_t]$, the time-varying across sequences can be represented as:

$$f_{d1} : \tilde{x}_t^i = A_t \cdot \tilde{x}_{t-1}^i + B_t + \gamma_t \tag{14}$$

$$f_{d2} : \tilde{x}_t^i = C_t \cdot \tilde{x}_{t-1}^i + D_t \cdot \tilde{x}_{t-2}^i + E_t + \gamma_t \tag{15}$$

where the model parameters $\beta_t^1 = [A_t, B_t]$ and $\beta_t^2 = [C_t, D_t, E_t]$ are all time-varying parameters and determined by data-fitting. γ_t is a time-dependent white noise representing the dynamics of stochasticity.

The first-order dynamics can be expressed as:

$$\left(\frac{\partial L(\tilde{\mathbf{x}}^i)}{\partial \tilde{x}_{t-1}^i}\right)_{d1} = \frac{\partial L(\tilde{\mathbf{x}}^i)}{\partial \tilde{x}_{t-1}^i} + \frac{\partial L(\tilde{\mathbf{x}}^i)}{\partial \tilde{x}_t^i} \cdot A_t \tag{16}$$

Similarly, second-order dynamics can be expressed as below by chain rule:

$$\left(\frac{\partial L(\tilde{\mathbf{x}}^i)}{\partial \tilde{x}_{t-2}^i}\right)_{d2} = \frac{\partial L(\tilde{\mathbf{x}}^i)}{\partial \tilde{x}_{t-2}^i} + \frac{\partial L(\tilde{\mathbf{x}}^i)}{\partial \tilde{x}_{t-1}^i} \cdot C_{t-1} + \frac{\partial L(\tilde{\mathbf{x}}^i)}{\partial \tilde{x}_t^i} \cdot (D_t + C_t \cdot C_{t-1}) \tag{17}$$

where $C_t = \frac{\partial \tilde{x}_t^i}{\partial \tilde{x}_{t-1}^i}$ and $D_t = \frac{\partial \tilde{x}_t^i}{\partial \tilde{x}_{t-2}^i}$. After computing $\tilde{x}_{t-1}^i = C_{t-1} \cdot \tilde{x}_{t-2}^i + D_{t-1} \cdot \tilde{x}_{t-3}^i + E_{t-1} + \gamma_{t-1}$, we can compute $C_{t-1} = \frac{\partial \tilde{x}_{t-1}^i}{\partial \tilde{x}_{t-2}^i}$.

4 Experiments

4.1 Experimental Settings

(A) Datasets and Evaluated Models. We choose three widely adopted skeletal datasets: HDM05 [26], NTU 60 [29] and NTU 120 [21]. We choose not only the most popular ST-GCN [44] as surrogate models but also the state-of-the-art classifiers including MS-G3D [23] and CTR-GCN [5]. For target models, apart from the above models, we also employ the recently proposed 2s-AGCN [31] and FR-HEAD [47]. In addition, we test the attack performance against defense models BEAT [39] and TRADES [45], which all demonstrate their robustness for action recognizers. Our appended model is a simple two-layer fully-connected layer network. Unless specified otherwise, we use $K = 3$ and $M = 20$ in Eq. (13) for default and explain the reason in the ablation study later. More implementation details are introduced in the **supplementary material**. *(B) Compared Attackers.* We compare our proposed PDBA with state-of-the-art attackers designed for S-HAR: SMART [40] and SMI [24]. We also adopt the commonly used transfer-based methods, including I-FGSM [16] and MI-FGSM [9]. For comparison with ensemble-based attacks, we choose recently proposed Ensemble [9] and SVRE [43]. We also compare our method with the state-of-the-art Bayesian attack BA [18]. For a fair comparison, we ran 200 iterations under l_∞ norm-bounded perturbation of size 0.01 for all attacks.

4.2 The Evaluation of Untargeted Attack

We first compare our method with baseline methods, including I-FGSM [16], MI-FGSM [9], SMART [40] and SMI [24]. The results are reported in Tab. 1. While current methods succeed in skeletal white-box/no-box attacks or image transfer-based attacks, they all struggle in transfer-based attacks on S-HAR. In contrast, our proposed PDBA achieves the highest average transfer success rate of **36.1%** across different models and datasets, surpassing SMART(the best baseline in S-HAR) and MI-FGSM (the strong transfer-based attack) by a margin of **26.8%** and **26.7%** respectively. Moreover, PDBA shows consistent transferability across all surrogate models, target models and datasets. These improvements break the common belief that transfer-based attacks in S-HAR suffer from low success rates and highly rely on the chosen surrogate [24, 39].

PDBA benefits from the Bayesian treatment on the appended models, thus we compare it with state-of-the-art ensemble-based methods. The comparisons provided in Tab. 2 include ensemble methods ENSEMBLE [9], SVRE [43] and Bayesian methods BA [18]. PDBA outperforms Ensemble and SVRE by a large margin and surpasses BA in most cases. Note that ENSEMBLE and SVRE know the full knowledge of ST-GCN, while ours treats ST-GCN as a black-box, hence it is very natural for ENSEMBLE and SVRE to achieve a higher attack success rate against ST-GCN. However, unlike the average gradient of ensemble models decreasing the white-box attack strength, PDBA consistently achieves almost **100%** attack success. We note that BA outperforms ENSEMBLE and

Table 1: The attack success rate(%) of untargeted transfer-based attacks on HDM05, NTU 60 and NTU 120. "Average" was calculated as the average transfer success rate over all victim models except for the surrogate.

Dataset	Surrogate	Method	Target					Average
			ST-GCN	2s-AGCN	MS-G3D	CTR-GCN	FR-HEAD	
HDM05	ST-GCN	I-FGSM	**99.06**	1.56	1.88	2.50	2.19	2.03
		MI-FGSM	96.88	2.29	6.04	2.71	2.29	3.33
		SMART	98.75	2.50	2.92	2.92	3.12	2.87
		SMI	97.79	2.45	6.62	3.19	2.94	3.80
		PDBA(Ours)	97.30	**14.26**	**60.54**	**37.50**	**23.43**	**33.93**
	MS-G3D	I-FGSM	5.00	1.88	97.18	3.75	2.50	3.28
		MI-FGSM	11.31	2.38	87.50	3.87	3.27	5.21
		SMART	7.50	2.19	96.25	3.44	3.44	4.14
		SMI	6.86	2.21	89.71	2.30	2.45	3.46
		PDBA(Ours)	**51.23**	**34.81**	**100.00**	**44.85**	**20.59**	**37.87**
NTU60	ST-GCN	I-FGSM	**100.00**	5.31	2.81	4.69	7.50	5.08
		MI-FGSM	97.92	5.95	2.68	7.44	7.44	5.88
		SMART	93.28	5.62	2.19	6.88	7.19	5.47
		SMI	90.63	3.43	2.69	6.62	6.62	4.84
		PDBA(Ours)	99.01	**52.45**	**70.13**	**22.18**	**53.46**	**49.56**
	MS-G3D	I-FGSM	15.63	7.81	**100.00**	7.50	9.38	10.08
		MI-FGSM	20.14	11.01	90.18	8.93	11.90	13.00
		SMART	21.66	8.96	**100.00**	12.50	13.54	14.17
		SMI	14.05	5.88	79.17	7.19	8.17	8.82
		PDBA(Ours)	**37.58**	**53.92**	**100.00**	**25.16**	**49.02**	**41.42**
NTU120	ST-GCN	I-FGSM	**100.00**	4.38	4.06	9.02	11.87	7.33
		MI-FGSM	95.54	8.93	7.44	12.20	13.10	10.42
		SMART	94.06	8.28	7.66	11.09	10.16	9.30
		SMI	62.50	4.41	4.41	6.62	8.82	6.07
		PDBA(Ours)	**100.00**	**19.60**	**14.48**	**15.20**	**22.79**	**18.02**
	MS-G3D	I-FGSM	29.37	11.25	**100.00**	15.31	16.25	18.05
		MI-FGSM	28.87	12.50	88.99	16.07	17.86	18.83
		SMART	31.25	13.96	**100.00**	16.04	17.92	19.79
		SMI	21.89	6.21	83.33	11.11	12.75	12.99
		PDBA(Ours)	**38.56**	**42.48**	**100.00**	**27.45**	**34.31**	**35.70**

SVRE. As a Bayesian method similar to PDBA, BA can smoothen the loss landscape by employing Bayesian models as surrogates (the landscape of BA is depicted in supplementary material). The results further demonstrate the correlation between loss landscape and adversarial transferability on S-HAR. However, unlike BA, which samples the full model distribution, PDBA treats the pre-trained surrogate as a black-box and only models the posterior of the appended model, thereby reducing computational overhead and speeding up the training process. More importantly, BA's overall attack performance is weaker than PDBA, regardless of whether in white-box or black-box settings.

4.3 The Evaluation of Targeted Attack

In this section, we focus on targeted attacks under the black-box setting. Improving transferability on S-HAR attack presents a greater challenge compared

Table 2: Comparsions with ensemble-based methods. ENSEMBLE and SVRE employ ST-GCN, MS-G3D and DGNN [30] as an ensemble of surrogate models. For the Bayesian-based methods BA and PDBA, we choose MS-G3D. "Average" was calculated as the average transfer success rate overall victim models except for the surrogate.

Dataset	Method	Target					Average
		ST-GCN	2s-AGCN	MS-G3D	CTR-GCN	FR-HEAD	
HDM05	ENSEMBLE	61.25	3.54	25.21	5.21	3.96	4.24
	SVRE	**86.46**	5.42	51.46	6.67	4.37	5.49
	BA	45.83	**38.75**	96.88	43.99	16.46	36.26
	PDBA(Ours)	51.23	34.81	**100.00**	**44.85**	**20.59**	**37.87**
NTU60	ENSEMBLE	54.49	17.57	50.58	11.13	19.14	15.95
	SVRE	**65.43**	26.76	48.63	9.38	23.63	19.92
	BA	30.10	43.10	99.61	24.40	47.25	36.21
	Ours	37.58	**53.92**	**100.00**	**25.16**	**49.02**	**41.42**
NTU120	ENSEMBLE	**72.66**	15.63	39.84	11.72	14.06	13.80
	SVRE	71.88	20.31	48.96	11.98	14.58	15.62
	BA	37.11	**49.61**	98.82	25.78	**37.50**	**37.50**
	PDBA(Ours)	38.56	42.48	**100.00**	**27.45**	34.31	35.70

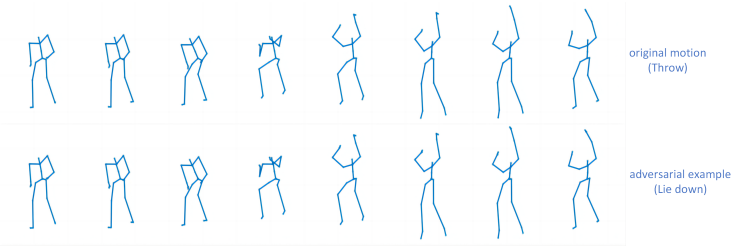

Fig. 3: The ground truth label **'Throw'** can be misclassified as **'Lie down'** on targeted attack by PDBA. The semantic differences between ground truth labels and target labels are large.

to untargeted attacks, remaining an open problem. This is primarily due to the significant semantic differences between the randomly selected class and the original one. Attacking a 'running' motion to 'walking' is generally easier than to 'drinking'. This is why targeted attacks have a lower success rate than untargeted attacks. However, Tab. 3 shows PDBA still outperforms the baseline under most scenarios. Moreover, PDBA can successfully attack the original class to a target with an obvious semantic gap without being detected by humans. A visual example can be found in Fig. 3.

4.4 The Evaluation on Defense Models

As BEAT shows high robustness against skeletal white-box attack [39], it is also interesting to evaluate the adversarial transferability of PDBA against it. We also employ the adversarial training method TRADES [45] as a baseline due to its effectiveness in S-HAR [8,39]. As shown in Tab. 4, PDBA achieves the highest attack success rate among the compared methods against defense models, which further validates its effectiveness.

Table 3: The targeted attack success rate (%) of targeted transfer-based attack on NTU60. "Average" was calculated as the average transfer success rate over all four victim models except for the surrogate.

Surrogate	Method	Target					Average
		ST-GCN	2s-AGCN	MS-G3D	CTR-GCN	FR-HEAD	
ST-GCN	MI-FGSM	**30.04**	3.63	2.32	4.94	4.13	3.76
	SMART	22.23	4.61	4.49	4.49	4.38	4.49
	PDBA(Ours)	28.79	**6.06**	**6.06**	**8.33**	**6.82**	**6.82**
MS-G3D	MI-FGSM	5.78	4.17	48.25	5.24	4.17	4.84
	SMART	7.14	8.04	**57.58**	8.35	8.35	7.97
	Ours	**9.09**	**9.09**	**57.58**	**9.85**	**9.33**	**9.34**
CTR-GCN	MI-FGSM	8.06	8.06	4.63	**43.34**	6.85	6.90
	SMART	5.44	5.14	5.44	27.92	5.75	5.44
	Ours	**8.33**	**9.09**	**8.33**	22.73	**9.09**	**8.71**
2s-AGCN	MI-FGSM	9.67	55.04	3.83	9.67	7.06	7.56
	SMART	4.95	54.60	**5.18**	5.18	5.65	5.24
	PDBA(Ours)	**10.61**	**76.52**	4.56	**10.61**	**8.33**	**8.53**

Table 4: The attack success rate (%) against defense model TRADES on HDM05 (top) and BEAT on NTU 60 (bottom)

Surrogate	Method	Untarget Attack			Target Attack		
		ST-GCN	MS-G3D	CTR-GCN	STGCN	MS-G3D	CTR-GCN
ST-GCN	MI-FGSM	3.33	3.33	2.71	6.88	**6.88**	**7.08**
	SMART	2.81	3.13	1.88	1.46	1.67	1.67
	PDBA(Ours)	**3.92**	**4.17**	**2.94**	**7.39**	6.82	6.82
MS-G3D	MI-FGSM	2.98	2.98	3.57	9.68	9.48	9.48
	SMART	2.50	3.13	3.13	1.25	1.46	1.46
	PDBA(Ours)	**12.26**	**10.29**	**12.25**	**10.61**	**11.36**	**11.36**
ST-GCN	MI-FGSM	68.45	2.98	8.33	24.69	2.21	4.84
	SMART	84.38	2.81	4.69	15.89	4.49	4.49
	PDBA(Ours)	**98.05**	**57.81**	**19.58**	**28.03**	**7.58**	**8.33**
MS-G3D	MI-FGSM	22.02	79.46	9.23	5.51	45.50	5.51
	SMART	17.19	98.75	6.56	6.69	53.57	8.04
	PDBA(Ours)	**36.27**	**99.67**	**23.86**	**9.09**	**60.61**	**9.85**

4.5 Ablation Study

Dual MCMC Sampling PDBA proposes a new dual MCMC sampling in the post-train Bayesian formulation(Eq. (13)). To see its contribution, we conduct an ablation study on the number of appended models (M and K in Eq. (13)). As shown in Tab. 5, compared with vanilla Post-train Bayesian strategy (M=0), the dual sampling significantly improves the attack performance. Furthermore, although PDBA theoretically requires intensive sampling for inference, in practice, we find a small number of sampling is sufficient ($K = 3$ and $M = 20$). More sampling will cause extra computation overhead. So we use $K = 3$ and $M = 20$ by default.

Motion Gradient In Sec. 3.3, PDBA benefits from the interplay between motion gradient (MG) and Bayesian manner. We hence conduct ablation stud-

Table 5: Ablation Study on NTU 60 with ST-GCN as the surrogate. M and K are the number dual MCMC sampling in Eq. (13). To isolate the impact of the number of appended models, we employ PDBA without motion gradient. The contribution of the motion gradient will be discussed in the subsequent ablation experiment.

K	M	Target				
		ST-GCN	2s-AGCN	MS-G3D	CTR-GCN	FR-HEAD
1	0	97.46	39.06	58.39	**19.53**	43.75
	10	**98.24**	40.23	**60.35**	19.14	45.31
	20	98.05	**41.21**	59.57	18.36	**45.72**
3	0	97.46	39.25	56.45	19.34	43.16
	10	98.07	42.01	60.57	19.73	**46.49**
	20	**98.75**	**43.75**	**60.98**	**20.57**	45.05
5	0	**97.92**	36.21	56.77	18.75	41.92
	10	96.88	**41.15**	**63.80**	16.93	45.05
	20	97.14	39.84	60.94	**20.57**	**45.21**

ies(MG/No MG) to show the effects of motion gradient and report the results in Tab. 6. Compared with PDBA without using motion gradient, PDBA with motion gradient consistently improves the attack success rate in both white box and transfer-based attacks, which shows the benefit of bringing the motion gradient into the Bayesian formulation.

Table 6: The ablation experiments of motion gradient. 'MG' means PDBA with motion gradient, 'No MG' means PDBA without using motion gradient.

Dataset	Surrogate	Method	Target				
			ST-GCN	2s-AGCN	MS-G3D	CTR-GCN	FR-HEAD
HDM05	ST-GCN	No MG	96.81	13.23	58.58	**38.97**	17.89
		MG	**97.30**	**14.26**	**60.54**	37.50	**23.43**
	MS-G3D	No MG	46.88	28.13	**100.00**	43.75	**21.88**
		MG	**51.23**	**34.81**	**100.00**	**44.85**	20.59
NTU60	ST-GCN	No MG	98.75	43.75	60.18	20.57	45.05
		MG	**99.01**	**52.45**	**70.13**	**22.18**	**53.46**
	MS-G3D	No MG	36.60	48.69	100.00	24.51	46.08
		MG	**37.58**	**53.92**	**100.00**	**25.16**	**49.02**
NTU120	ST-GCN	No MG	98.53	**20.83**	**24.46**	14.71	21.81
		MG	**100.00**	19.60	14.48	**15.20**	**22.79**
	MS-G3D	No MG	34.64	36.27	100.00	25.49	32.03
		MG	**38.56**	**42.48**	**100.00**	**27.45**	**34.31**

4.6 Surrogate Transferability

A common belief is transfer-based attacks in S-HAR are sensitive to chosen surrogates [24, 39, 40]. In this subsection, we conduct a detailed analysis of the factors contributing to this phenomenon. As illustrated in Tab. 7, CTR-GCN, in general, shows relatively high transferability across various attack methods. Notably, our findings reveal that CTR-GCN manifests smoother regions within

the loss landscape (see Fig. 1), in contrast to the more rugged terrain observed with ST-GCN. Considering that our method largely improves transferability by further flattening the rugged landscape, we suspect that model smoothness plays a pivotal role in boosting adversarial transferability for S-HAR, potentially outweighing the significance of gradient-based optimization techniques. Next, MS-G3D has better transferability than ST-GCN. Unlike ST-GCN, which solely extracts joint information, MSG3D explicitly incorporates the bone information, thereby effectively capturing the relative movements of joints. In conclusion, we recommend that skeletal transfer-based attacks employ smoother two-stream surrogates incorporating both joint and bone information.

Table 7: The untargeted attack success rate (%) with different surrogate models in NTU60 for additional discussions.

Surrogate	Method	Target				
		ST-GCN	2s-AGCN	MS-G3D	CTR-GCN	FR-HEAD
ST-GCN	MI-FGSM	97.92	5.95	2.68	7.44	7.44
	SMART	93.28	5.62	2.19	6.88	7.19
	PDBA	**99.01**	52.45	70.13	22.18	53.46
MS-G3D	MI-FGSM	20.14	11.01	90.18	8.93	11.90
	SMART	21.66	8.96	**100.00**	12.50	13.54
	PDBA	37.58	53.92	**100.00**	25.16	49.02
CTR-GCN	MI-FGSM	15.21	7.59	7.50	99.17	20.21
	SMART	15.00	5.00	4.69	99.69	15.31
	PDBA	33.20	**65.65**	75.15	**100.00**	**59.77**

5 Limitation and Conclusion

We propose a novel Post-train Dual Bayesian Attack (PDBA), which effectively explores the model posterior space for a collection of surrogates with high adversarial transferability on S-HAR. Additionally, PDBA incorporates information of the motion dynamics into the attack gradient in a Bayesian manner. More broadly, PDBA extends the Bayesian attack family by introducing a new post-train Bayesian strategy. One limitation is that the improvement for targeted transfer-based attacks is not as obvious as untargeted transfer-based attack, despite surpassing existing methods. However, we argue that PDBA signifies a substantial advancement in skeletal transfer-based attacks, particularly when considering the struggles faced by existing methods in this domain. Nonetheless, boosting the targeted transferability is still an open problem and we will explore this further in the future.

References

1. Ali, A., Pinyoanuntapong, E., Wang, P., Dorodchi, M.: Skeleton-based human action recognition via convolutional neural networks (cnn). arXiv preprint arXiv:2301.13360 (2023) 4

2. Blundell, C., Cornebise, J., Kavukcuoglu, K., Wierstra, D.: Weight uncertainty in neural network. In: International conference on machine learning. pp. 1613–1622. PMLR (2015) 3
3. Brendel, W., Rauber, J., Bethge, M.: Decision-based adversarial attacks: Reliable attacks against black-box machine learning models. arXiv preprint arXiv:1712.04248 (2017) 4
4. Bringmann, L.F., Hamaker, E.L., Vigo, D.E., Aubert, A., Borsboom, D., Tuerlinckx, F.: Changing dynamics: Time-varying autoregressive models using generalized additive modeling. Psychological methods **22**(3), 409 (2017) 8
5. Chen, Y., Zhang, Z., Yuan, C., Li, B., Deng, Y., Hu, W.: Channel-wise topology refinement graph convolution for skeleton-based action recognition. In: Proceedings of the IEEE/CVF international conference on computer vision. pp. 13359–13368 (2021) 3, 9
6. Dai, C., Huang, Y., Chien, W.C.: A sparse attack method on skeleton-based human action recognition for intelligent metaverse application. Future Generation Computer Systems **143**, 51–60 (2023) 4
7. Diao, Y., Shao, T., Yang, Y.L., Zhou, K., Wang, H.: Basar:black-box attack on skeletal action recognition. In: Proceedings of the IEEE/CVF Conference on Computer Vision and Pattern Recognition (CVPR). pp. 7597–7607 (June 2021) 1, 3, 4
8. Diao, Y., Wang, H., Shao, T., Yang, Y.L., Zhou, K., Hogg, D.: Understanding the vulnerability of skeleton-based human activity recognition via black-box attack. arXiv preprint arXiv:2211.11312 (2022) 11
9. Dong, Y., Liao, F., Pang, T., Su, H., Zhu, J., Hu, X., Li, J.: Boosting adversarial attacks with momentum. In: Proceedings of the IEEE Conference on Computer Vision and Pattern Recognition (CVPR) (June 2018) 3, 4, 9
10. Du, Y., Wang, W., Wang, L.: Hierarchical recurrent neural network for skeleton based action recognition. In: Proceedings of the IEEE conference on computer vision and pattern recognition. pp. 1110–1118 (2015) 4
11. Goodfellow, I.J., Shlens, J., Szegedy, C.: Explaining and harnessing adversarial examples. arXiv preprint arXiv:1412.6572 (2014) 1
12. Goodfellow, I.J., Shlens, J., Szegedy, C.: Explaining and harnessing adversarial examples. arXiv preprint arXiv:1412.6572 (2014) 4
13. Gubri, M., Cordy, M., Papadakis, M., Le Traon, Y., Sen, K.: Efficient and transferable adversarial examples from bayesian neural networks. In: Uncertainty in Artificial Intelligence. pp. 738–748. PMLR (2022) 3, 4, 5
14. Izmailov, P., Podoprikhin, D., Garipov, T., Vetrov, D., Wilson, A.G.: Averaging weights leads to wider optima and better generalization. arXiv preprint arXiv:1803.05407 (2018) 7
15. Kang, Z., Xia, H., Zhang, R., Jiang, S., Shi, X., Zhang, Z.: Fgda-gs: Fast guided decision attack based on gradient signs for skeletal action recognition. Computers & Security **135**, 103522 (2023) 4
16. Kurakin, A., Goodfellow, I.J., Bengio, S.: Adversarial examples in the physical world. In: Artificial intelligence safety and security, pp. 99–112. Chapman and Hall/CRC (2018) 9
17. Li, H., Xu, Z., Taylor, G., Studer, C., Goldstein, T.: Visualizing the loss landscape of neural nets. Advances in neural information processing systems **31** (2018) 2
18. Li, Q., Guo, Y., Zuo, W., Chen, H.: Making substitute models more bayesian can enhance transferability of adversarial examples. In: The Eleventh International Conference on Learning Representations, ICLR 2023, Kigali, Rwanda, May 1-5, 2023 (2023), https://openreview.net/pdf?id=bjPPypbLre 3, 4, 5, 6, 7, 9

19. Lin, J., Song, C., He, K., Wang, L., Hopcroft, J.E.: Nesterov accelerated gradient and scale invariance for adversarial attacks. arXiv preprint arXiv:1908.06281 (2019) 4
20. Liu, J., Akhtar, N., Mian, A.: Adversarial attack on skeleton-based human action recognition. IEEE Transactions on Neural Networks and Learning Systems **33**(4), 1609–1622 (2020) 2, 4
21. Liu, J., Shahroudy, A., Perez, M., Wang, G., Duan, L.Y., Kot, A.C.: Ntu rgb+ d 120: A large-scale benchmark for 3d human activity understanding. IEEE transactions on pattern analysis and machine intelligence **42**(10), 2684–2701 (2019) 5, 9
22. Liu, Y., Chen, X., Liu, C., Song, D.: Delving into transferable adversarial examples and black-box attacks. In: International Conference on Learning Representations (2016) 2
23. Liu, Z., Zhang, H., Chen, Z., Wang, Z., Ouyang, W.: Disentangling and unifying graph convolutions for skeleton-based action recognition. In: Proceedings of the IEEE/CVF conference on computer vision and pattern recognition. pp. 143–152 (2020) 4, 9
24. Lu, Z., Wang, H., Chang, Z., Yang, G., Shum, H.P.H.: Hard no-box adversarial attack on skeleton-based human action recognition with skeleton-motion-informed gradient. In: Proceedings of the IEEE/CVF International Conference on Computer Vision (ICCV). pp. 4597–4606 (October 2023) 2, 3, 4, 5, 9, 13
25. Maddox, W.J., Izmailov, P., Garipov, T., Vetrov, D.P., Wilson, A.G.: A simple baseline for bayesian uncertainty in deep learning. Advances in neural information processing systems **32** (2019) 3, 7
26. Müller, M., Röder, T., Clausen, M., Eberhardt, B., Krüger, B., Weber, A.: Mocap database hdm05. Institut für Informatik II, Universität Bonn **2**(7) (2007) 9
27. Qin, Z., Fan, Y., Liu, Y., Shen, L., Zhang, Y., Wang, J., Wu, B.: Boosting the transferability of adversarial attacks with reverse adversarial perturbation. Advances in Neural Information Processing Systems **35**, 29845–29858 (2022) 1, 3, 4
28. Ren, B., Liu, M., Ding, R., Liu, H.: A survey on 3d skeleton-based action recognition using learning method. Cyborg and Bionic Systems (2020) 2, 4
29. Shahroudy, A., Liu, J., Ng, T.T., Wang, G.: Ntu rgb+ d: A large scale dataset for 3d human activity analysis. In: Proceedings of the IEEE conference on computer vision and pattern recognition. pp. 1010–1019 (2016) 9
30. Shi, L., Zhang, Y., Cheng, J., Lu, H.: Skeleton-based action recognition with directed graph neural networks. In: Proceedings of the IEEE/CVF conference on computer vision and pattern recognition. pp. 7912–7921 (2019) 4, 11
31. Shi, L., Zhang, Y., Cheng, J., Lu, H.: Two-stream adaptive graph convolutional networks for skeleton-based action recognition. In: Proceedings of the IEEE/CVF conference on computer vision and pattern recognition. pp. 12026–12035 (2019) 4, 9
32. Springenberg, J.T., Klein, A., Falkner, S., Hutter, F.: Bayesian optimization with robust bayesian neural networks. Advances in neural information processing systems **29** (2016) 7
33. Springer, J., Mitchell, M., Kenyon, G.: A little robustness goes a long way: Leveraging robust features for targeted transfer attacks. Advances in Neural Information Processing Systems **34**, 9759–9773 (2021) 6
34. Szegedy, C., Zaremba, W., Sutskever, I., Bruna, J., Erhan, D., Goodfellow, I., Fergus, R.: Intriguing properties of neural networks. arXiv preprint arXiv:1312.6199 (2013) 4

35. Tanaka, N., Kera, H., Kawamoto, K.: Adversarial bone length attack on action recognition. In: Proceedings of the AAAI Conference on Artificial Intelligence. vol. 36, pp. 2335–2343 (2022) 2, 3, 4
36. Tanaka, N., Kera, H., Kawamoto, K.: Fourier analysis on robustness of graph convolutional neural networks for skeleton-based action recognition. Computer Vision and Image Understanding **240**, 103936 (2024) 2, 4
37. Tang, X., Wang, H., Hu, B., Gong, X., Yi, R., Kou, Q., Jin, X.: Real-time controllable motion transition for characters. ACM Transactions on Graphics (TOG) **41**(4), 1–10 (2022) 8
38. Wang, H., Diao, Y.: Defending black-box classifiers by bayesian boundary correction. arXiv preprint arXiv:2306.16979 (2023) 7
39. Wang, H., Diao, Y., Tan, Z., Guo, G.: Defending black-box skeleton-based human activity classifiers. In: Williams, B., Chen, Y., Neville, J. (eds.) Thirty-Seventh AAAI Conference on Artificial Intelligence, AAAI 2023, Thirty-Fifth Conference on Innovative Applications of Artificial Intelligence, IAAI 2023, Thirteenth Symposium on Educational Advances in Artificial Intelligence, EAAI 2023, Washington, DC, USA, February 7-14, 2023. pp. 2546–2554. AAAI Press (2023). https://doi.org/10.1609/AAAI.V37I2.25352, https://doi.org/10.1609/aaai.v37i2.25352 5, 9, 11, 13
40. Wang, H., He, F., Peng, Z., Shao, T., Yang, Y.L., Zhou, K., Hogg, D.: Understanding the robustness of skeleton-based action recognition under adversarial attack. In: Proceedings of the IEEE/CVF Conference on Computer Vision and Pattern Recognition. pp. 14656–14665 (2021) 1, 2, 3, 4, 9, 13
41. Wu, L., Zhu, Z.: Towards understanding and improving the transferability of adversarial examples in deep neural networks. In: Asian Conference on Machine Learning. pp. 837–850. PMLR (2020) 1, 3
42. Xia, S., Wang, C., Chai, J., Hodgins, J.: Realtime style transfer for unlabeled heterogeneous human motion. ACM Transactions on Graphics (TOG) **34**(4), 1–10 (2015) 8
43. Xiong, Y., Lin, J., Zhang, M., Hopcroft, J.E., He, K.: Stochastic variance reduced ensemble adversarial attack for boosting the adversarial transferability. In: Proceedings of the IEEE/CVF Conference on Computer Vision and Pattern Recognition. pp. 14983–14992 (2022) 4, 9
44. Yan, S., Xiong, Y., Lin, D.: Spatial temporal graph convolutional networks for skeleton-based action recognition. In: Proceedings of the AAAI conference on artificial intelligence. vol. 32 (2018) 3, 4, 9
45. Zhang, H., Yu, Y., Jiao, J., Xing, E., El Ghaoui, L., Jordan, M.: Theoretically principled trade-off between robustness and accuracy. In: International conference on machine learning. pp. 7472–7482. PMLR (2019) 9, 11
46. Zhang, Y., Hu, S., Zhang, L.Y., Shi, J., Li, M., Liu, X., Jin, H.: Why does little robustness help? a further step towards understanding adversarial transferability. In: Proceedings of the 45th IEEE Symposium on Security and Privacy (S&P'24). vol. 2 (2024) 6
47. Zhou, H., Liu, Q., Wang, Y.: Learning discriminative representations for skeleton based action recognition. In: Proceedings of the IEEE/CVF Conference on Computer Vision and Pattern Recognition (CVPR). pp. 10608–10617 (June 2023) 4, 9